Kovove Mater. 59 2021 131–139
DOI: 10.4149/km_2021_2_131

Interfacial microstructure and fractography of Ti6Al4V/5A05Al dissimilar joint using the cold arc MIG welding

S. Wei[1]*, W. Rao[2]

[1] *School of Materials Science and Engineering, North University of China, Taiyuan 030051, P. R. China*
[2] *School of Energy and Power Engineering, North University of China, Taiyuan 030051, P. R. China*

Received 28 September 2020, received in revised form 30 November 2020, accepted 1 March 2021

Abstract

Titanium Ti6Al4V and aluminum 5A05Al were cold arc MIG welded using Al-Si5 filler. The feasibility of Ti/Al dissimilar cold arc MIG welding-brazing was investigated by microstructure examination and fractography. Welds without defects were fabricated; however, the Ti/Al interface exhibited non-uniform structures. A multilayered structure, including an α-Ti layer, a $TiAl_3$ + Ti_5Si_3 mixed layer, and a serrate $TiAl_3$ layer, was observed in the upper regions. In comparison, only a thin cellular $TiAl_3$ layer was observed in other regions. Two types of fracture modes, including a ductile fracture mode and a mixed brittle-ductile fracture mode, were observed in a single joint. The ultimate tensile strength of the Ti/Al joints surpassed 240 MPa.

K e y w o r d s: dissimilar joining, cold arc welding, welding-brazing, microstructure, fractography

1. Introduction

Light-weight structures have environmental and economic significance. Ti/Al hybrid structure has been drawing attention to its potential applications in the aviation and space industries. The possible usages of Ti/Al structures in fuselage areas, such as aircraft seat tracks and jet engine leading-edge nacelle inlet, were given in [1–3]. However, previous research suggested that the significant mismatch in physical properties and the intrinsic embrittlement of Ti-Al intermetallic compounds (IMCs) are the main problems encountered in Ti/Al conventional thermal joining [4]. These two unfavorable factors could eventually result in the initiation and propagation of welding cracks [5]. To overcome these adverse effects, the welding-brazing process was brought in and was proved efficient in improving the joint strength. Subsequent research was conducted using laser beam welding (LBW) [2, 4] and tungsten inert gas (TIG) welding [6, 7]. Being highly efficient and low cost, metal inert gas (MIG) welding is another attractive choice in Ti/Al welding-brazing. A few attempts were carried out using MIG welding, and some progress was made [8–14].

As [15] and [16] stated that the element Si was efficient in restricting the formation of Ti-Al IMCs, Al-Si wires (Al-Si5 or Al-Si12) were selected as the fillers in most of the researches. A series of attempts on Ti/Al dissimilar joining were done using pulsed current MIG (P-MIG) welding by the authors [8–10]; the Al-Si5 wire was the selected filler. The interrelationship between interfacial microstructure and welding heat input was investigated in [9], the joining mechanism between titanium and aluminum was discussed in [10]. Despite the fact that few satisfactory welds were obtained, the potential usage of the MIG welding in Ti/Al dissimilar welding-brazing was demonstrated.

Up to now, a few researches were done with the concern of Ti/Al dissimilar MIG welding-brazing. The cold metal transfer (CMT) welding technology was utilized in lap welding-brazing of Ti/Al dissimilar joint. Comparative analysis of the Ti/Al interface and tensile strength with different configuration forms was done in [11]. An external axial magnetic field hybrid

*Corresponding author: tel.: +86 351 3557519; e-mail address: wszweishouzheng@126.com

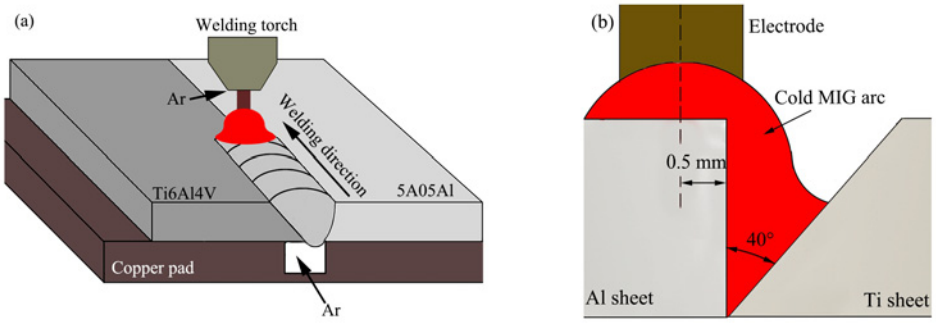

Fig. 1. The schematic diagrams for the welding process (a) and for the wire offset (b).

Table 1. Chemical composition for Ti, Al, and filler wire (wt.%)

Elements	Ti	Al	V	Si	Fe	Mg	Cu	Zn	Mn	C	N	H	O
Ti6Al4V	Bal.	5.5–6.8	3.5–4.5	≤ 0.15	≤ 0.30	–	–	–	–	≤ 0.1	≤ 0.05	≤ 0.01	≤ 0.20
5A05Al	–	Bal.	–	0.5	0.5	4.8–5.5	0.1	0.2	0.3–0.6	–	–	–	–
ER4043 wire	≤ 0.2	Bal.	–	5.5	≤ 0.8	≤ 0.05	≤ 0.3	≤ 0.1	≤ 0.05	–	–	–	–

CMT welding process was used in further research; the interfacial microstructures and joint properties under the influence of the magnetic field were discussed [12]. A bypass-current MIG welding technology was used to join AA6061/Ti6Al4V dissimilar alloys with Al-Si5 filler; the maximum tensile-shear strength of the lap joints reached 190 MPa [13]. A wire and arc additive manufacturing (WAAM) technology was chosen in welding-brazing of Ti-6Al-4V/Al-6.25Cu dissimilar joint. However, the joint properties were still not satisfying [14]. All the referenced studies above were focused on Ti/Al lap joining; the Ti/Al butt MIG joining has been rarely studied but by the authors. Thus butt MIG welding-brazing of Ti/Al dissimilar joint needs further studying, scientific analysis of the Ti/Al interfacial features and the fracture behavior should be conducted.

The cold arc MIG (CA-MIG) welding technology, invented by EWM High Technology Co., Ltd. (Germany), has the characteristic of controlling heat input accurately. As reported in [17], the power source could provide a much lower heat input without reducing the arc stability. To avoid the melting of titanium and suppressing the excessive formation of Ti-Al IMCs, CA-MIG welding has technical advantages. So far, few published studies concerning Ti/Al dissimilar CA-MIG welding have been retrieved. The CA-MIG welding technology was adopted in Ti6Al4V/5A05Al dissimilar butt joining in the present work. The application of low heat input aimed to prevent the fusion of titanium. The investigations on interfacial microstructures and joint properties aimed to verify the feasibility of Ti/Al dissimilar CA-MIG welding. The fracture modes of the joint were also discussed.

2. Experimental procedure

The titanium Ti6Al4V and aluminum 5A05Al sheets with the dimensions of 150 × 100 × 2.5 mm^3 were used as the base metals. Mechanical grinding and chemical cleaning were applied to the sheets' surfaces to remove oxide films and oil contamination. A mixed acid solution with the volume ratio of $HNO_3 : HF : H_2O = 10 : 1 : 39$ was used to wash the titanium sheets for 3 min. Chemical cleaning, including alkaline cleaning and acid pickling, was applied to the aluminum sheets in the standard order. The areas near the weld seam were further cleaned using a high-speed rotating wire brush before welding. Al-Si wires were used in most previous attempts; thus Al-Si5 wire (ø 1.2 mm, Indalco Alloys Co., Ltd., Canada) was used in the present work. Table 1 gives the compositions of titanium, aluminum, and filler wire.

The Alpha Q351 CA-MIG welding system (EWM High Technology Co., Ltd., Germany) was used as the welding source. A pulsed current cold arc MIG welding mode (No. 60 marked on the device) was selected, and the welding process was conducted at room temperature without flux. High purity argon (99.999 vol.%) was used as the shielding gas; the seam was double-sided protected.

The control design for the welding process is shown in Fig. 1. The butt configuration was adopted in the different welding experiments (Fig. 1a). To increase the interfacial bonding area, a single groove was fabricated in titanium with a bevel angle of about 40°. To prevent the mass formation of brittle Ti-Al IMCs, the electrode was set to point to the aluminum with a 0.5 mm offset from the seam center. The schematic diagram for the wire offset is shown in Fig. 1b. The filler

Table 2. Main parameters for the CA-MIG welding

Average welding current I (A)	Average arc voltage U (V)	Welding speed v (m min^{-1})	Flow rate of shielding gas v_g (l min^{-1})		Welding heat input E (kJ cm^{-1})
			top	back	
90 ± 3	15 ± 0.2	0.6	20	15	1.29–1.41

wire was fed automatically with the feeding rate of 5.2 m min^{-1}. The selection of the welding parameters was based on former attempts [18]; the main parameters are listed in Table 2.

All the weldments were free placed for at least 24 h to ensure the accuracy of the following tests. The joint appearance and the joint cross-section view were captured to evaluate the joint formability. Cross-sectional metallographic specimens were prepared following standard procedures and etched in mixed acid (HF 15 vol.%, HNO_3 15 vol.%, and H_2O 70 vol.%). The X-Ray diffraction (XRD) analysis was conducted near the Ti/Al interface to determine the phases; the analysis angle was in the range of 20° ∼100°. Microstructure features of the Ti/Al interfaces at different regions were examined using a JSM-7001F FE-SEM system (JEOL Co., Ltd., Japan) equipped with an Inca X-Max^N EDS (Oxford Instruments Co., Ltd., UK).

The Instron-5569 universal mechanical testing machine (Instron Co., Ltd., USA) was used in the tensile tests; the strain rate was 6.7 × 10^{-4} s^{-1}. Three test specimens were cut from the weldment; then, they were fabricated into a gauge size of 200 × 10 × 2.5 mm^3 without removing the reinforcement. Control tensile test was conducted using untreated aluminum base metal to evaluate the joint strength. Fractography was conducted using FE-SEM and EDS analysis.

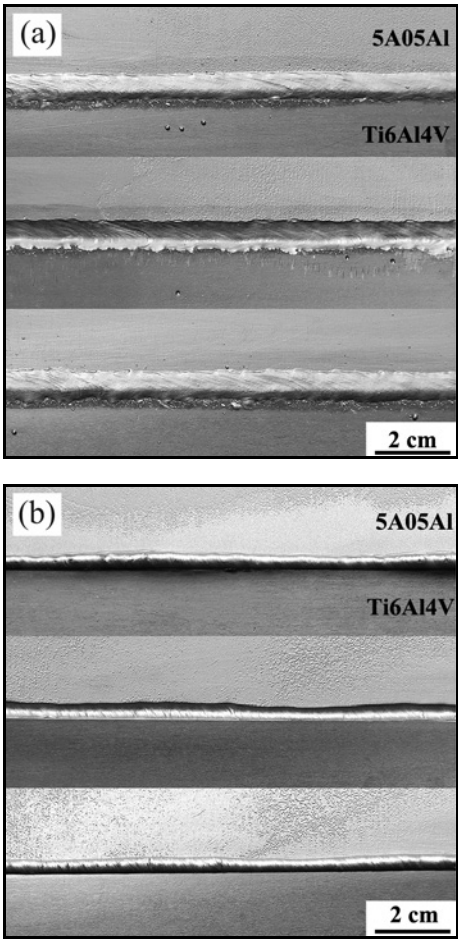

Fig. 2. Top (a) and back (b) appearances of the joints.

3. Results and discussion

3.1. Formability of the joints

Three weldments were randomly selected, top and back appearances for the joints were captured, as shown in Fig. 2. The visual inspection of the joints globally revealed a satisfactory aspect. Full-penetration welds were obtained by using the operational parameters. Neither cracks nor blow holes were observed in the weld surface.

The upper weld surfaces are smooth, and the weld widths are in the range of 7 ± 1 mm (Fig. 2a). As the welding process was carried out with low heat input, the evaporation of liquid mixed metals was weak. Only a small amount of spatters was observed on the titanium sheets. The back welds exhibit a satisfactory appearance, which can be attributed to the good wettability and spreadability of the liquid Al-Si filler. Smooth and uniform back welds with width of 3 ± 0.5 mm were observed, as shown in Fig. 2b.

Typical joint cross-sections were cut from the weldments using EDM wire cutting, as shown in Fig. 3. According to Fig. 3a, the Ti/Al interfaces were sharp and clear. It is reasonable to infer that the titanium sheets stayed in a solid state during the welding or were infinitesimally melted.

The metallographic specimen was fabricated and then filmed using a digital camera, as shown in Fig. 3b. Under the operational conditions, all the titanium surfaces were well wetted by the liquid mixed metal, and

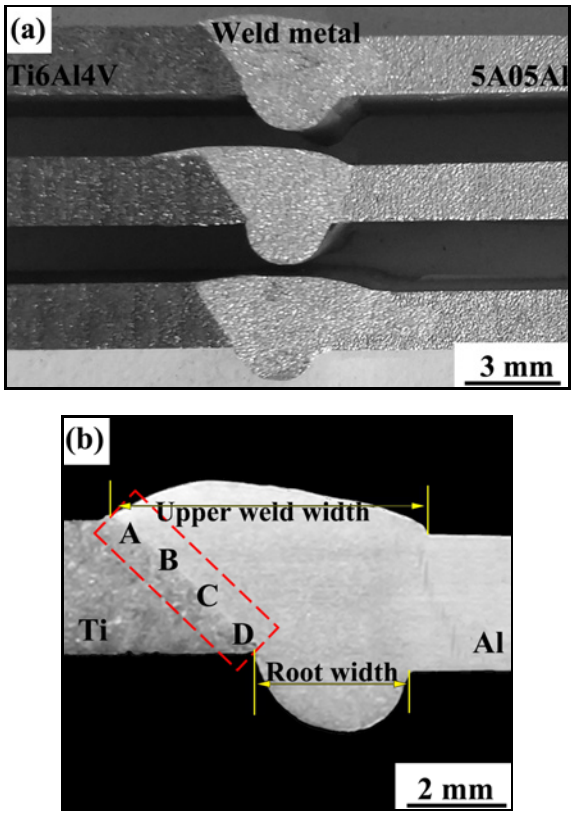

Fig. 3. Cross-sections of the joints (a) and the metallographic specimen (b).

satisfying top and back profiles were obtained. Moreover, favorable transition zones were formed on the aluminum side. It is receivable to infer that the aluminum sheets were partially melted during the welding. Fusion zones were developed thanks to the temperature gradient and composition gradient near the solid-liquid interface. As the V-shaped groove was fabricated in titanium, the weld bead was formed into a funnel shape. The root reinforcement volume is a bit large thanks to the offset of the welding arc toward aluminum and the liquid filler's high fluidity. The upper weld width is approximately 7 mm, while the root width is about 3 mm.

3.2. Microstructures of Ti/Al interface

The phase constitution of the joint cross-section was tested using XRD. The rough specimen was cut off as marked with a dotted red rectangle in Fig. 3b; the long side of the rectangle was parallel to the Ti/Al interface. To get the full analysis of the possible phases, the as-tested aspect was ground to a mirror-like finish. The XRD profile for the weld zone is shown in Fig. 4. IMCs $TiAl_3$ and Ti_5Si_3 were identified.

As reported in [19], an unfavorable problem faced with Ti/Al dissimilar joining is the interfacial reaction

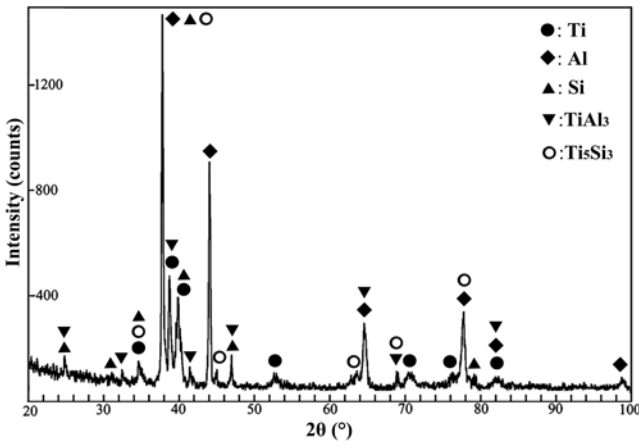

Fig. 4. XRD patterns for the weld zone.

nonhomogeneity. Due to the non-uniform thermal field of the welding arc, the upper parts of the Ti/Al interface were heated directly by the blazing arc, while the bottom parts underwent a much lower heating effect. Besides, the gap was filled up by the liquid droplets in a bottom-up sequence; the bottom interface was sheltered from the arc continuous heating by the molten pool at a late stage of the welding. These two main factors consequently caused the difference in welding heat input at different regions.

The focus of the following study was on Ti/Al interfacial morphologies. The interface was characteristic of non-uniform structures. Microstructures of regions alphabetically marked A, B, C, and D in Fig. 3b were captured using FE-SEM and EDS. Figure 5 shows the microstructures for the selected regions. Based on the general observations, two different interfaces were formed because of the welding heat input difference. No thick reaction zone was observed in the sample, indicating that the titanium stayed in the solid state during the CA-MIG welding. The titanium and aluminum sheets were joined by a welding-brazing mechanism.

According to Figs. 5a and 5b, multilayered interfacial reaction zones were observed in both region A and region B. The reaction zone could be divided into three distinct layers. A gray layer with uniform thickness, a thin layer scattered with nanoparticles, and a serrated layer were formed orderly from the titanium side to the weld side. The result is in accordance with that observed in the former research [8].

Thanks to the direct heating effect from the welding arc, the weld heat input that these two parts underwent was relatively high. The duration time of high temperature (higher than the minimum reaction temperature) was a little longer. The interfacial reactions between titanium and liquid mixed metal lasted for sufficient time to form favorable reaction zones. Because of the offset of the MIG arc toward aluminum

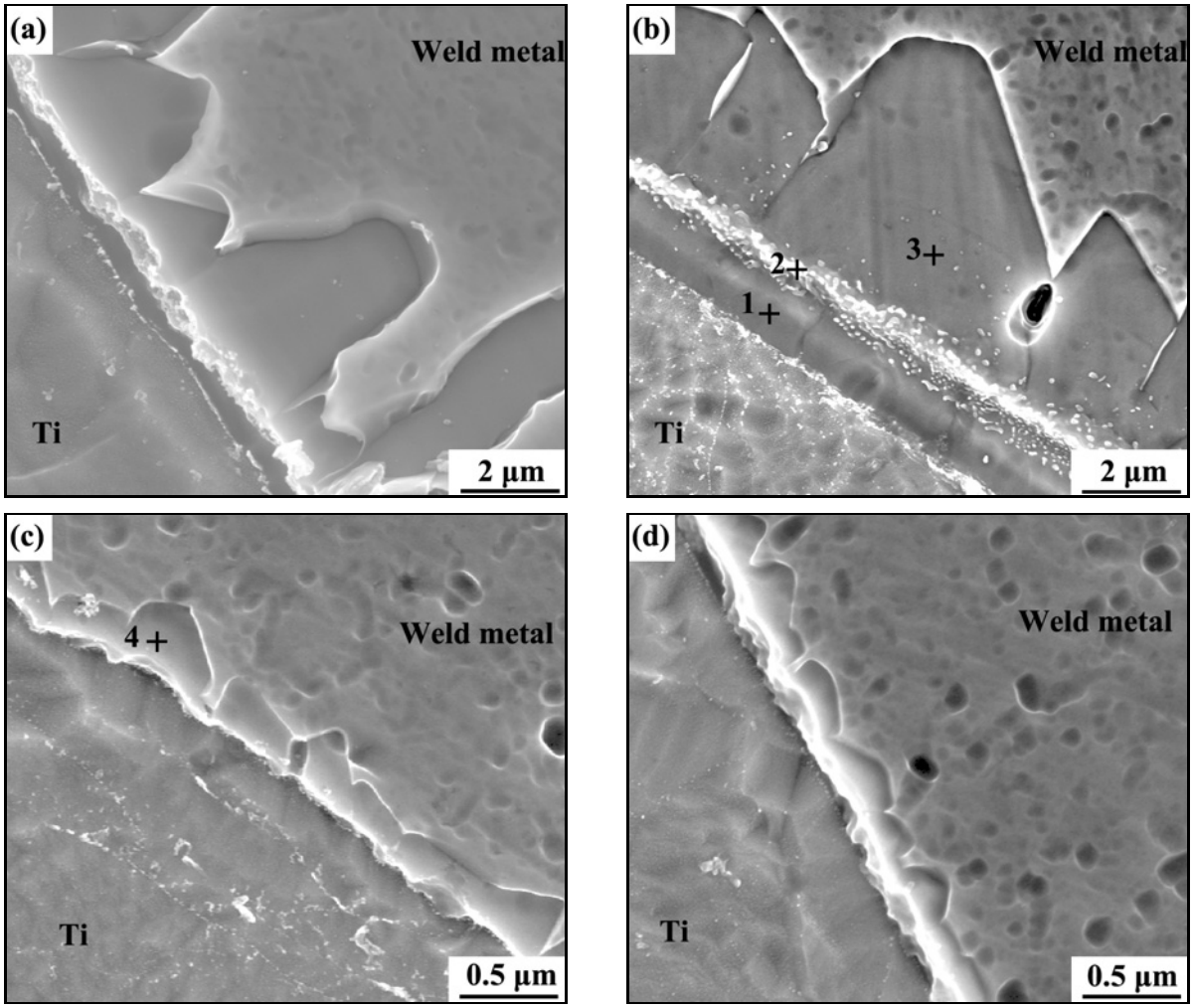

Fig. 5. The interfacial microstructures for locations A–D in Fig. 3b.

and the single groove in titanium, the weld heat input of region B was higher than that of region A. Thereby, the reaction zone at the top 1/3 part is a little thicker than that at the top part. The average thickness of the reaction zone at region A is approximately 3 μm, while at region B, the thickness increased to about 5 μm.

For the bottom 1/3 part and the root part (Figs. 5c and 5d), with a lack of direct heating by the welding arc, the weld heat input that these parts underwent was low. Compared with upper parts, the interfacial reactions lasted for a much shorter time. Only a cellular layer with a thickness of about 0.3 μm was observed.

To fully understand the reaction zones, the following discussion was focused on the phase constitutions of the interfaces. As two types of interfaces are observed, chemical compositions of selected regions marked 1–4 (in Figs. 5b and 5c) were determined using EDS. For the regions with higher heat input, the atomic ratio of Ti in the uniform layer reaches 83.68 at.% (Fig. 6a), which is much more than the 13.34 at.% for Al. The layer is mostly composed of supersaturated α-Ti, as demonstrated in [20, 21]. A strong segregation of Si was observed in the layer scattered with tiny particles (Fig. 6b), the atomic ratio of Ti to Al is close to 1 : 2. According to the former calculation results in [20], the formation of Ti_5Si_3 particles is prior to Ti-Al IMCs because the reaction has a much lower Gibbs free energy change. Thus the tiny particles might be the IMC Ti_5Si_3; the layer might be the mixture of IMCs $TiAl_3$ + Ti_5Si_3 by considering the XRD results. The atomic ratio of Ti : Al is nearly equal to 1 : 3 in the serrated layer, so the layer is supposed to be composed of IMC $TiAl_3$ (Fig. 6c). IMC Ti_5Si_3 and $TiAl_3$ are the detected products, which is in accordance with the XRD profile. The formation of the granular $Ti_7Al_5Si_{12}$ phase was observed in a laser welded-brazed Ti/Al joint [22]. However, this ternary phase was undetected in the present study.

For the regions with low heat input (Figs. 5c and 5d), only one cellular reaction layer was observed. The chemical analysis revealed 68.89 at.% Al, 23.52 at.%

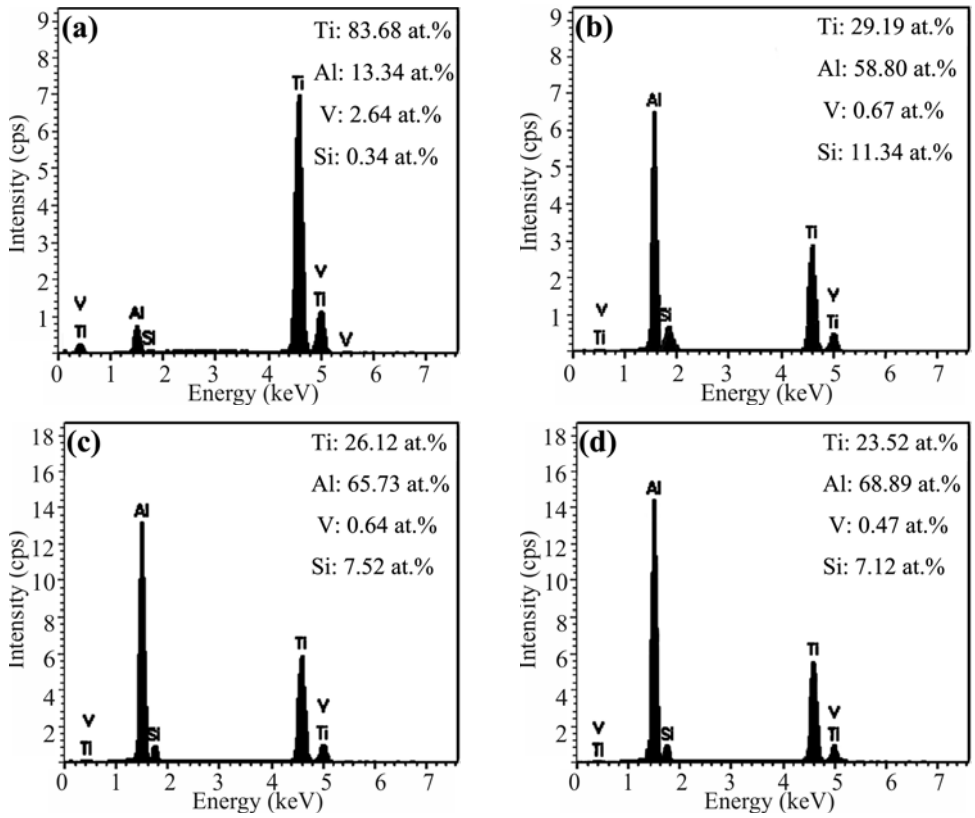

Fig. 6. EDS results for regions 1–4 in Fig. 5.

Ti, and 7.12 at.% Si (Fig. 6d). It is receivable to conclude that the layer is mostly the IMC $TiAl_3$. Based on the observations in [15], the formation temperature of IMC Ti_5Si_3 is higher than that of $TiAl_3$. The absence of the Ti_5Si_3 indicates that the peak temperature of these regions was higher than the formation temperature of $TiAl_3$, however, lower than that of Ti_5Si_3.

Despite the non-uniform interfacial microstructures, the Ti/Al interfacial bonding was integrated using the operational parameters. Based on the fact that cracks and porosities were absent near the Ti/Al interface, the joint properties might be high.

3.3. Mechanical properties and fracture analysis

Three test specimens were transversely cut from the weldment. The control sample was cut from the untreated aluminum sheets. Images for the fractured specimens are shown in Fig. 7; the joints were broken in two types of fracture modes. Only one sample was fractured in aluminum base metal (marked as fracture mode 1) thanks to the sound Ti/Al interfacial bonding. According to the top view and cross-sectional view, the fracture zone reveals remarkable plastic deformation and significant cross-section shrinkage. The other two samples were fractured in the weld (marked as fracture mode 2); the fracture happened mostly in

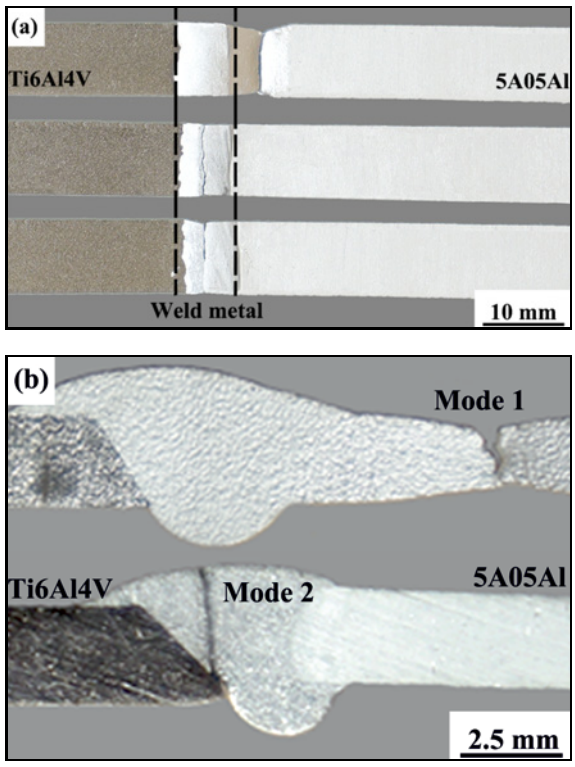

Fig. 7. Images of tensile tested samples (a) and fracture modes (b).

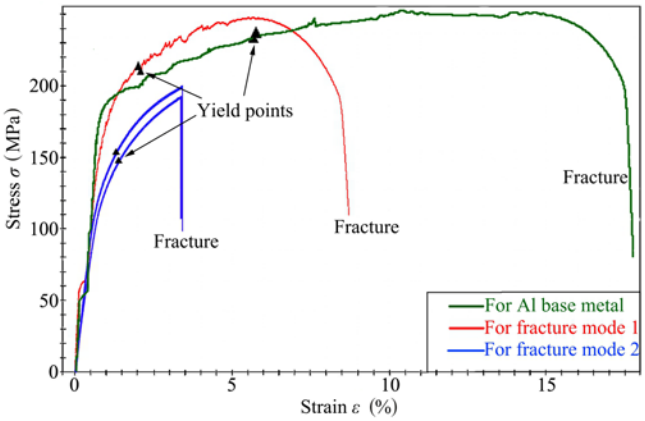

Fig. 8. Stress-strain curves for aluminum and Ti/Al joints.

the weld while broken at the interface near the weld root (Fig. 7b).

Figure 8 shows the stress-strain curves for all the test specimens. The green curve is for the untreated aluminum, the red curve is for the joint fractured in mode 1, and the other two are for joints fractured in mode 2. The values for yield strength were automatically determined by the built-in software. For the sample fractured in mode 1, a typical elastic-plastic deformation was observed. The yield strength is about 210 MPa, and the ultimate tensile strength (UTS) is 242.3 MPa, while for the control sample, the yield strength is 231.2 MPa and the UTS is about 251 MPa. The joint strength reduction might result from the microstructure changes and solution behavior in the heat affected zone. The strain of the sample is much lower than that of aluminum, which is approximately 7 %.

For the samples fractured in mode 2, the plastic deformation was small, and the strength values are much lower. The average yield strength was approximately 150 MPa, and the average UTS was about 192 MPa, respectively. The strain values of the two samples are close to each other, which is about 3.4 %.

Fractography examination of the specimens was carried out to understand the fracture mechanism. Fractography for the sample broken in aluminum is shown in Fig. 9a, the ductile fracture mechanism was revealed. The fractured surface could be divided into a fibrous zone, a radial zone, and a shear lip zone. The fracture mechanism has already become common sense and will not be further discussed.

The global view of the fractured surface for fracture mode 2 (Fig. 9b), which was broken in the weld metal, shows two distinct zones: one is rich in Al, the other is rich in Ti. The morphology of the Al-rich zone is shown in Fig. 9c. The area full of the sharp tearing ridge was demonstrated to be α-Al solution by EDS analysis (Al 99.34 wt.%, Si 0.66 wt.%). Intergranular fracture mode was observed in particular regions; the chemical compositions (Al 85.47 wt.%, Si 14.53 wt.%) are in accordance with the Al + Si eutectic structure. A small number of blowholes were observed, as shown in Fig. 9d. By cutting down the cross-sectional area, the porosity likely was

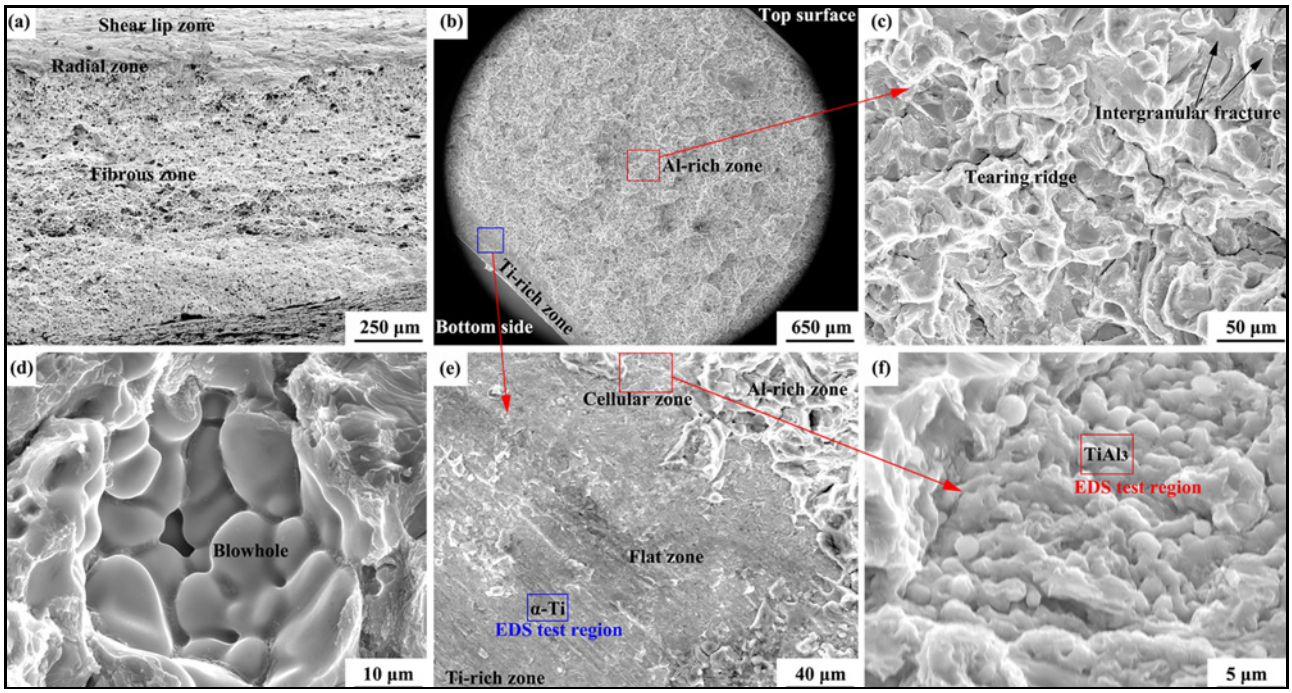

Fig. 9. Fractography for fracture mode 1 (a) and for fracture mode 2 (b)–(f).

one of the factors responsible for reducing the joint strength.

The Ti-rich zone is located at the root part; the morphology is shown in Fig. 9e. The titanium surface suffered from weak adherence of weld metal; the interfacial bonding was inefficient. The fractured surface, overall, was flat and was supposed to be broken in brittle fracture mode. The EDS chemical compositions of the flat zone were Ti 91.15 wt.%, Al 8.62 wt.%, Si 0.23 wt.%. It is reasonable to infer that the zone was mostly broken at the interface between the $TiAl_3$ layer and titanium. Except for the flat zone, a narrow cellular zone was observed adjacent to the interface between the Ti-rich zone and Al-rich zone, which was marked with a red box in Fig. 9e. The cellular structure was examined using EDS and was demonstrated to be the IMC $TiAl_3$ (Fig. 9f). The results supposed the cellular zone to be broken at the interface between the $TiAl_3$ layer and the weld metal. Rare, tiny tearing ridges were observed in the cellular zone, which indicates that the toughness of the zone was higher than that of the flat zone.

Based on the observations above, the fracture mechanism for fracture mode 2 can be summarized into three stages:

(i) The crack initiated at the weld root due to stress concentration and weak interfacial bonding. According to observations in [5], the bond strength of the $Ti/TiAl_3$ interface might be weaker than that of the $Al/TiAl_3$ interface; the main crack mostly propagated along the $Ti/TiAl_3$ interface. Owing to the region's low toughness, a brittle fracture happened, and a flat zone was formed.

(ii) As demonstrated in [23], the propagation of the main crack was hindered by the cellular $TiAl_3$ at the area with a thicker $TiAl_3$ layer. The crack was forced to propagate along the $TiAl_3/Al$ interface, and a cellular fracture zone was formed.

(iii) The further propagation of the crack encountered the thick serrated $TiAl_3$ layer, and the crack tip swerved into the weld metal. The toughness of the weld metal was severely reduced by the brittle intergranular Al + Si eutectic structure and the blowholes. The joint eventually fractured in the weld metal under the uniaxial tensile stress.

4. Conclusions

The study confirmed the feasibility of CA-MIG welding-brazing of Ti/Al dissimilar joint. The welding-brazing mechanism was confirmed based on the fact that the titanium had stayed in the solid state during the welding. Well-formed joints were fabricated by using the operational parameters. However, heterogeneity of the Ti/Al interfacial microstructure was observed. For the regions with high welding heat input, an α-Ti layer, a $TiAl_3$ + Ti_5Si_3 mixed layer, and a serrated $TiAl_3$ layer were observed. In comparison, only a thin cellular $TiAl_3$ layer was observed in the regions with low heat input.

Two fracture modes were observed during the tensile test. For the specimen fractured in aluminum base metal, a typical ductile fracture mode was observed, and the UTS reached 242.3 MPa. Other samples were fractured in a mixed brittle-ductile fracture mode; the fracture happened at the root Ti/Al interface firstly and then extended into the weld metal. The average tensile strength for the latter fracture mode was lower than 200 MPa. The weak Ti/Al interfacial bonding at the weld root and the porosity in the weld metal were responsible for the reduction of the joint strength.

Acknowledgements

This research was financially supported by the National Natural Science Foundation of China (No. 51805492) and the Natural Science Foundation of Shanxi Province (No. 201801D221149). The authors express heartfelt thanks here.

References

[1] M. Kreimeyer, F. Wagner, F. Vollertsen, Laser processing of aluminum-titanium-tailored blanks, Opt. Laser Eng. 43 (2005) 1021–1035. doi:10.1016/j.optlaseng.2004.07.005

[2] F. Moller, C. Thomy, F. Vollertsen, Joining of titanium-aluminium seat tracks for aircraft applications – system technology and joint properties, Weld. World 56 (2012) 108–114. doi:10.1007/BF03321341

[3] D. Sanders, P. Edwards, G. Grant, M. Ramulu, A. Reynolds, Superplastically formed friction stir welded tailored aluminum and titanium blanks for aerospace applications, J. Mater. Eng. Perform. 19 (2010) 515–520. doi:10.1007/s11665-010-9617-1

[4] W. V. Vaidya, M. Horstmann, V. Ventzke, B. Petrovski, M. Kocak, R. Kocik, G. Tempus, Improving interfacial properties of a laser beam welded dissimilar joint of aluminium AA6056 and titanium Ti6Al4V for aeronautical applications, J. Mater. Sci. 45 (2010) 6242–6254. doi:10.1007/s10853-010-4719-6

[5] S. Wei, Y. Li, J. Wang, K. Liu, Research on cracking initiation and propagation near Ti/Al interface during TIG welding of titanium to aluminum, Kovove Mater. 52 (2014) 85–91. doi:10.4149/km_2014_2_85

[6] K. Nandagopal, C. Kailasanathan, Analysis of mechanical properties and optimization of gas tungsten arc welding (GTAW) parameters on dissimilar metal titanium (6Al-4V) and aluminium 7075 by Taguchi and ANOVA techniques, J. Alloy Comp. 682 (2016) 503–516. doi:10.1016/j.jallcom.2016.05.006

[7] H. Wang, X. Yuan, T. Li, K. Wu, Y. Sun, C. Xu, TIG welding-brazing of Ti6Al4V and Al5052 in overlap configuration with assistance of zinc foil, J. Mater. Process. Techn. 251 (2018) 26–36. doi:10.1016/j.jmatprotec.2017.08.015

[8] S. Wei, Y. Li, J. Wang, K. Liu, P. Zhang, Microstructure characteristics of Ti-2Al-Mn/Al1060 dissimilar joint by pulsed gas metal arc welding-brazing, Kovove Mater. 52 (2014) 305–311. doi:10.4149/km_2014_5_305

[9] S. Wei, Y. Li, J. Wang, K. Liu, Influence of welding heat input on microstructure of Ti/Al joint during pulsed gas metal arc welding, Mater. Manuf. Process. 29 (2014) 954–960. doi:10.1080/10426914.2014.880464

[10] S. Wei, Y. Li, J. Wang, K. Liu, P. Zhang, Microstructure and joining mechanism of Ti/Al dissimilar joint by pulsed gas metal arc welding, Int. J. Adv. Manuf. Technol. 70 (2014) 1137–1142. doi:10.1007/s00170-013-5290-5

[11] J. Li, Q. Sun, Y. Liu, Ch. Cai, J. Feng, Cold metal transfer welding-brazing of pure titanium TA2 to aluminum alloy 6061-T6, Adv. Eng. Mater. 19 (2017) 1600494. doi:10.1002/adem.201600494

[12] Q. J. Sun, J. Z. Li, Y. B. Liu, B. P. Li, P. W. Xu, J. C. Feng, Microstructural characterization and mechanical properties of Al/Ti welded by CMT method--assisted hybrid magnetic field, Mater. Design 116 (2017) 316–324. doi:10.1016/j.matdes.2016.12.025

[13] Y. Miao, Z. Ma, X. Yang, J. Liu, D. Han, Experimental study on microstructure and mechanical properties of AA6061/Ti-6Al-4V joints made by bypass-current MIG welding-brazing, J. Mater. Process. Techn. 260 (2018) 104–111. doi:10.1016/j.jmatprotec.2018.05.019

[14] Y. Tian, J. Shen, S. Hu, J. Guo, E. Kannatey-Asibu, Wire and arc additive manufactured Ti-6Al-4V/Al--6.25Cu dissimilar alloys by CMT-welding: Effect of deposition order on reaction layer, Sci. Technol. Weld. Join. 25 (2020) 73–80. doi:10.1080/13621718.2019.1629379

[15] P. G. Shant, Intermetallic compounds in diffusion couples of Ti with an Al-Si eutectic alloy, Mater. Charact. 49 (2003) 321–330. doi:10.1016/S1044-5803(02)00342-X

[16] S. H. Chen, L. Q. Li, Y. B. Chen, D. J. Liu, Si diffusion behavior during laser welding-brazing of Al alloy and Ti alloy with Al-12Si filler wire, T. Nonferr. Metal. Soc. 20 (2010) 64–70. doi:10.1016/S1003-6326(09)60098-4

[17] P. Kah, R. Suoranta, J. Martikainen, Advanced gas metal arc welding processes, Int. J. Adv. Manuf. Technol. 97 (2013) 655–674. doi:10.1007/s00170-012-4513-5

[18] S. Wei, W. Rao, Z. Li, Y. Zhang, Cold arc MIG welding of titanium Ti6Al4V to aluminum 5A05Al using Al-Mg5 filler, Met. Mater. Int. 26 (2020) 1555–1561. doi:10.1007/s12540-019-00402-3

[19] S. Chen, L. Li, Y. Chen, J. Dai, J. Huang, Improving interfacial reaction non-homogeneity during laser welding-brazing aluminum to titanium, Mater. Design 32 (2011) 4408–4416. doi:10.1016/j.matdes.2011.03.074

[20] S. Wei, Y. Li, J. Wang, K. Liu, Formation of brittle phases during pulsed current gas tungsten arc welding of titanium to aluminum alloys, J. Mater. Eng. Perform. 23 (2014) 1451–1457. doi:10.1007/s11665-014-0874-2

[21] S. Wei, Y. Li, J. Wang, K. Liu, Improving of interfacial microstructure of Ti/Al joint during GTA welding by adopting pulsed current, Int. J. Adv. Manuf. Technol. 73 (2014) 1307–1312. doi:10.1007/s00170-014-5929-x

[22] S. Chen, L. Li, Y. Chen, J. Huang, Joining mechanism of Ti/Al dissimilar alloys during laser welding--brazing process, J. Alloy Compd. 509 (2011) 891–898. doi:10.1016/j.jallcom.2010.09.125

[23] Y. Chen, S. Chen, L. Li, Influence of interfacial reaction layer morphologies on crack initiation and propagation in Ti/Al joint by laser welding-brazing, Mater. Design 31 (2010) 227–233. doi:10.1016/j.matdes.2009.06.029